Anticorrelation between temperature and fluctuations of the switching current in moderately damped Josephson junctions

V. M. Krasnov and T. Golod

Department of Physics, Stockholm University, Albanova University Center, SE-10691 Stockholm, Sweden

T. Bauch and P. Delsing

Department of Microtechnology and Nanoscience, Chalmers University of Technology, SE-41296 Göteborg, Sweden

We study the influence of dissipation on the switching current statistics of moderately damped Josephson junctions. Different types of both low- and high-T_c junctions with controlled damping are studied. The damping parameter of the junctions is tuned in a wide range by changing temperature, magnetic field, and gate voltage and introducing a ferromagnetic layer or *in situ* capacitive shunting. A paradoxical collapse of switching current fluctuations with increasing T occurs in all studied junctions. The phenomenon critically depends on dissipation in the junction and is explained by the interplay of two counteracting consequences of thermal fluctuations, which, on one hand, assist in premature switching into the resistive state and, on the other hand, help in retrapping back to the superconducting state. This is one of the rare examples of anticorrelation between temperature and the amplitude of fluctuations of a physically measurable quantity.

I. INTRODUCTION

Temperature is a measure of the energy of thermal fluctuations. For example, it is well known that noise in electronic components or Brownian motion of small particles increase with temperature. However, does the amplitude of fluctuations of physical properties always increase with T? Recently, a spectacular exception from this rule was reported almost simultaneously by three groups of researchers.[1–3] It was observed that fluctuations of the bias current required for switching of a Josephson junction (JJ) from the superconducting (S) to the resistive (R) state may suddenly collapse (drastically decrease) at elevated T. It was suggested that the paradoxical behavior is caused by the fact that temperature does not only provide energy for excitation of a system from the equilibrium state but also enhance the rate of relaxation back to the equilibrium. The latter strongly depends on the damping in the system and, under certain circumstances, can reverse the correlation between fluctuations and temperature.

Dissipation plays a crucial role in decay of metastable states, which determines the dynamics of various physical and chemical processes.[4,5] Switching between S and R states in JJ's is one of the best studied examples of such a decay. The influence of dissipation on the switching statistics of JJ's has been intensively studied both theoretically[4,6–9] and experimentally.[10–15] The role of dissipation in decoherence of quantum systems has been widely discussed[16] and has recently become an important issue for quantum computing. JJ's are used in several different ways in qubit implementations. For example, current biased JJ's are employed in phase qubits,[17] where the dissipation affects relaxation and decoherence in the qubits. Furthermore, switching of JJ's is also used for readout of both flux[18] and charge-phase[19] qubits.

Here, we present an extensive study of dissipation effects on the phase dynamics in moderately damped JJ's. For this purpose, we prepared several types of junctions with well controlled and tunable damping parameters. In particular, we study low Ohmic Nb-Pt-Nb superconductor–normal-metal–superconductor (SNS) junctions, Nb-CuNi-Nb superconductor—ferromagnet-superconductor (SFS) junctions with a diluted ferromagnetic alloys, and Nb-InAs-Nb superconductor—two-dimensional-electron-gas–superconductor (S-2DEG-S) junctions, as well as $Bi_2Sr_2CaCu_2O_{8+\delta}$ (Bi-2212) high-T_c superconductor (HTSC) intrinsic JJ's. The influence of dissipation on thermal and quantum fluctuations is studied by tuning damping parameters of the junctions by temperature, magnetic field, and gate voltage and, introducing a ferromagnetic layer or capacitive shunting. The paradoxical collapse of switching current fluctuations with increasing T was observed in all cases. It is shown that the collapse temperature critically depends on dissipation in the junction. The phenomenon is explained by interplay of two conflicting consequences of thermal fluctuations, which, on one hand, assist in premature switching to the resistive state and, on the other hand, help in retrapping back to the superconducting state. The conclusions are supported by analytical calculations and numerical simulations, which are in quantitative agreement with experimental data presented here as well as with those reported in Refs. 1–3.

The paper is organized as follows. In Sec. II, we summarize the results of the resistively and capacitively shunted junction (RCSJ) model, required for the analysis of switching statistics in moderately damped JJ's. In Sec. III, we characterize the JJ's studied in this work and describe the experimental techniques. In Sec. IV, we analyze the magnetic field modulation of the switching and retrapping currents. This helps us understand the origin of hysteresis in the current-voltage characteristics (IVC's) and estimate the damping parameters of our JJ's. In Sec. V, the main experimental results on the switching current statistics are presented. It is shown that the collapse of switching current fluctuations occurs in all moderately damped JJ's and that the macroscopic quantum tunneling (MQT) phenomena persist even in strongly

damped SNS-type JJ's. Finally, in Sec. VI, we discuss the mechanism of the paradoxical collapse and present numeric and analytic calculations, which clarify the phase dynamics in the collapsed state and support our conclusions.

II. GENERAL RELATIONS

The damping parameter of JJ's within the RCSJ model is characterized by the inverse value of the quality factor at zero bias current, Q_0. For junctions with sinusoidal current-phase relation (CPR), it is given by

$$Q_0 = \omega_{p0}RC = \sqrt{2eI_{c0}R^2C/\hbar}. \tag{1}$$

Here, $\omega_{p0} = (2eI_{c0}/\hbar C)^{1/2}$ is the Josephson plasma frequency at zero bias, R and C are the junction resistance and capacitance, respectively, and I_{c0} is the fluctuation-free critical current. Determination of Q_0 is not trivial: I_{c0} must be obtained by measurement and extrapolation of the switching current statistics,[11] the effective capacitance is not equal to the geometric one because leads form a sort of transmission line with finite inductance, and for superconductor-insulator-superconductor (SIS) tunnel junctions, the effective resistance is ill defined. The effective damping in SIS junctions is typically dominated by the high frequency impedance of circuitry, $\sim 100~\Omega$,[11] which can be up-transformed by the high dielectric constant substrate[20] but may also be affected by the quasiparticle resistance for junctions with smaller tunnel resistance and at elevated T. Furthermore, damping in SIS junctions is frequency and bias dependent due to the strong nonlinearity of the IVC's.

At finite bias current, the quality factor $Q(I)$ is given by the same Eq. (1) with ω_{p0} replaced by the Josephson plasma frequency at finite bias, which, for junctions with the sinusoidal CPR, is $\omega_p(I) = \omega_{p0}[1-(I/I_{c0})^2]^{1/4}$. This means that the quality factor is bias dependent, $Q(I) = Q_0[1-(I/I_{c0})^2]^{1/4}$. For SIS junctions, $Q(I)$ can be further reduced due to frequency dependence of R. Therefore, the phase dynamics may change from underdamped, $Q \gtrsim 1$, to overdamped, $Q \lesssim 1$, as $I \to I_{c0}$.

The electrodynamics of JJ's is equivalent to motion of a particle in a tilted washboard potential formed by superposition of the periodic Josephson potential and the work done by the current source (the tilt), as shown in Fig. 1. The particle can escape from the potential well as a result of MQT or thermal activation (TA) process. At low damping, the escaped particle will roll down the potential (switch to the R state). However, if dissipation exceeds the work done by the current source, it will be retrapped in subsequent wells and return to the S state, as shown in Fig. 1.

The TA escape rate from S to R state is determined by an Arrhenius law, and for moderate and high damping cases, it is given by[7]

$$\Gamma_{TA} = a_t \frac{\omega_p(I)}{2\pi} \exp\left[-\frac{\Delta U_S(I)}{k_B T}\right]. \tag{2}$$

Here, ΔU_S is the potential barrier for S-R switching, see Fig. 1, which, for the sinusoidal CPR, is
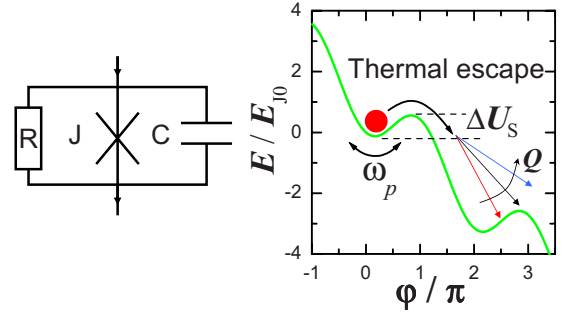

FIG. 1. (Color online) (Left) The equivalent circuit of the RCSJ model. (Right) The mechanical analog of the RCSJ model: the tilted wash board potential in the energy-phase space for $I=0.5I_{c0}$. Arrows indicate three possible particle trajectories after thermal escape for different quality factors. For the lowest Q, the particle get's retrapped in the next potential well, while for highest Q, it will continue to roll down the potential, leading to switching of the JJ from the superconducting to the resistive state.

$$\Delta U_S \simeq (4\sqrt{2}/3)E_{J0}[1-I/I_{c0}]^{3/2}, \tag{3}$$

where $E_{J0} = (\hbar/2e)I_{c0}$ is the Josephson energy. Damping enters only into the prefactor of Γ_{TA}:

$$a_t = (1+1/4Q^2)^{1/2} - 1/2Q. \tag{4}$$

The MQT escape rate can be written in notations of Ref. 8 as

$$\Gamma_{MQT} = \gamma(T)\frac{\omega_p}{2\pi}\left[\frac{\Delta U_S}{\hbar\omega_p}\right]^{1/2}\chi(Q)\exp\left[-\frac{\Delta U_S}{\hbar\omega_p}s(Q)\right]. \tag{5}$$

Here, $\gamma(T)$ is the thermal correction with the characteristic parabolic dependence $\ln\gamma \propto T^2$,[21] and in the case of strong damping, $\chi(Q) \simeq 2\pi\sqrt{3}Q^{7/2}\{1-Q^2[8\ln(2Q)-4.428]\}$ and $s(Q) \simeq 3\pi[Q+Q^{-1}]$.

The MQT rate can be strongly affected by dissipation since the damping dependent factor $s(Q)$ appears under the exponent in Eq. (5). Qualitatively, this is due to smearing of quantum levels in the washboard potential with decreasing Q. Indeed, the spacing between the lowest levels is $\sim\hbar\omega_p$, while the level width is $\sim\hbar/RC$. From Eq. (1), it follows that for $Q<1$, the width becomes larger than the separation between levels, which leads to suppression of the MQT.

In the moderate damping case, the crossover between MQT and TA occurs at[7]

$$T_{MQT}(Q) = \frac{\hbar\omega_p}{2\pi k_B}\left[\left(1+\frac{1}{4Q^2}\right)^{1/2} - \frac{1}{2Q}\right]. \tag{6}$$

From Eq. (6), it follows that the MQT-TA crossover temperature decreases with Q due to the general suppression of the MQT, as discussed above.

An analytic expression for the retrapping rate from the R to the S state is known only for strongly underdamped JJ's, $Q_0 \gg 1$ (Ref. 6):

$$\Gamma_R = \omega_{p0}\frac{I-I_{R0}}{I_{c0}}\sqrt{\frac{E_{J0}}{2\pi k_B T}}\exp\left[-\frac{\Delta U_R(I)}{k_B T}\right], \tag{7}$$

$$\Delta U_R \simeq \frac{E_{J0}Q_0^2}{2}\left[\frac{I - I_{R0}}{I_{c0}}\right]^2.$$ (8)

Here, I_{R0} is the fluctuation-free retrapping current and ΔU_R the retrapping (dissipation) barrier. From Eq. (8), it is seen that retrapping, unlike escape, depends strongly on damping,[15] because Q_0^2 appears under the exponent in Eq. (7). For underdamped JJ's, the I_{R0} is given by

$$I_{R0} \simeq \frac{4 I_{c0}}{\pi Q_0}.$$ (9)

This expression is valid for $Q_0 \gtrsim 3$. For smaller Q_0,

$$I_{R0}/I_{c0} \simeq 1.272\,99 - 0.311\,02 Q_0 - 0.029\,65 Q_0^2 + 0.013\,06 Q_0^3.$$ (10)

Equation (10) was obtained from interpolation of the numerically simulated IVC's within the RCSJ model.[22] This expression is valid for $0.84 \lesssim Q_0 < 3$. For $Q_0 \lesssim 0.84$, the IVC's are nonhysteretic, i.e., $I_{R0} = I_{c0}$.

A. Switching statistics

For a given switching rate Γ_{01} from the initial state 0 to state 1, the probability of switching within the infinitesimal time interval δt is given by $\mathbb{P}_{01}(\delta t) = \delta t \Gamma_{01}$. The probability of staying in the 0 state is $\mathbb{P}_0(\delta t) = 1 - \delta t \Gamma_{01}$. The probability of staying in the 0 state within a finite time interval t is then given by the conditional probability of not switching during all subintervals δt: $\mathbb{P}_0(t) = \lim_{\delta t \to 0}(1 - \delta t \Gamma_{01})^{t/\delta t} = \exp[-\Gamma_{01}t]$.[23]

Measurements of switching statistics in JJ's are performed by either ramping the bias current at constant rate dI/dt or by applying current pulses to the junction. The results presented below do not depend on the measuring technique, i.e., similar results were obtained by both ramping[2,3] and pulse[1] techniques. Since the switching rate $\Gamma_{01}(I)$ is bias dependent, the probability of not switching until current I in the current ramping experiment can be written as

$$\mathbb{P}_0(I) = \exp\left[-\frac{1}{dI/dt}\int_0^I \Gamma_{01}(I)dI\right].$$ (11)

Alternatively, it can be written as

$$\mathbb{P}_0(I) = 1 - \int_0^I P_{01}(I)dI,$$ (12)

where $P_{01}(I)$ is the probability density of switching from 0 to 1 state. By definition, $P_{01}(I)\delta I$ is the probability of switching in the bias interval from I to $I + \delta I$. The probability density is one of the most important characteristics of switching statistics because it directly corresponds to experimentally measured switching current histograms.

Differentiating Eqs. (11) and (12) with respect to I, we obtain

$$P_{01} = -\frac{d\mathbb{P}_0(I)}{dI} = \frac{\Gamma_{01}(I)}{dI/dt}\left(1 - \int_0^I P_{01}(I)dI\right).$$ (13)

This equation has a clear physical meaning: the probability of measuring the switching event in the current interval from I to $I + \delta I$ is the conditional probability of switching during the ramping time $\delta t = \delta I/(dI/dt)$ (first term) and the probability that the system has not already switched before (second term). The recurrent equation (13) is easily solved numerically and couples the switching probability density P_{01} to the switching rate Γ_{01}.

The probability density for switching from S to R state follows directly from Eq. (13), where 0 and 1 are S and R, states, respectively. To obtain the probability density of retrapping P_R from R to S state, we should take into account that current is now ramped downward to zero and that $P_R = 0$ at $I \geq I_{c0}$:

$$P_R(I) = \frac{\Gamma_R(I)}{|dI/dt|}\left[1 - \int_I^{I_{c0}} P_R(I)dI\right].$$ (14)

The probability of remaining in the R state and not being retrapped until current I is

$$\mathbb{P}_{nR}(I) = 1 - \int_I^{I_{c0}} P_R(I)dI.$$ (15)

Thermal fluctuations lead to premature switching and retrapping. This means that fluctuations tend to decrease the switching current I_S with respect to I_{c0} but increase the retrapping current I_R with respect to I_{R0}. Therefore, thermal fluctuations help in returning the JJ from R to S state. One should also keep in mind that since retrapping critically depends on damping and damping depends on bias, retrapping can become prominent at the switching current even for junctions which are underdamped at zero bias.

III. SAMPLES

Analysis of dissipation effects on phase dynamics requires junctions with well defined and controlled damping parameters. Ideally, such junctions should be of RCSJ type with bias independent R and have R much smaller than 100 Ω to avoid shunting by the high frequency impedance of the circuitry, $Z_0 \sim 100$ Ω. Previous studies of fluctuation phenomena in JJ's were performed predominantly on underdamped, $Q_0 \gg 1$, SIS tunnel junctions, which are not described by the simple RCSJ model with constant Q_0 both due to strongly nonlinear IVC's and considerable shunting by the high frequency impedance.[9] This ambiguity does not exist for SNS junctions, which are well described by RCSJ model with constant R, typically much smaller than Z_0.

Although the quality factor of SNS junctions is expected to be constant, verification of this, as well as exact evaluation of Q_0, is nontrivial. Parameters I_{c0} and C still need to be independently defined. Furthermore, Eq. (1) is valid only for junctions with sinusoidal CPR. The CPR in SNS junctions deviates from sinusoidal,[24] which changes the plasma frequency ω_{p0} and thus affects the effective C entering Eq. (1).

TABLE I. Summary of the studied junctions. Here, I_{c0} is the fluctuation free critical current, R is the normal resistance, T^* is the collapse temperature, and Q_0 is the quality factor at $I=0$.

Junction	Geometry	I_{c0} (μA)	R (Ω)	T^* (K)	$Q_0(T^*)$
		SFS (Nb/CuNi)			
1a	70/50 nm	770	0.24		
2a	25/50 nm	178	0.21	0.2[a]	1.0[a]
2b	25/50 nm	34	0.26		$\gtrsim$0.84
		S-2DEG-S (2DEG $w \times L$)			
1a	10 μm$\times$500 nm	2.5	36		~0.84
2b	40 μm$\times$400 nm	37	7.5	0.8	1.63
3a	10 μm$\times$500 nm	2.3	38.1		0.88
3b	40 μm$\times$500 nm	7.3	11.4	0.1	0.95
		C shunted			
3a	10 μm$\times$500 nm	2.5	34	0.45	2.4
3b	40 μm$\times$500 nm	7.4	10.3	>1	>3
SNS	170$\times$88 nm^2	262	0.6		<0.84
Bi-2212	4$\times$2.5 μm^2	125	~40	75	5.6

[a]At $H \simeq 0.5$ Oe.

The effective C is no longer equal to the real, explicitly measurable junction capacitance. Therefore, quantitative analysis of dissipation effects requires a possibility of tuning the quality factor by at least as many independent parameters as the amount of unknown variables in Eq. (1).

In this work, we focus on the analysis of phase dynamics in low Ohmic SNS-type junctions with moderate damping $1 \lesssim Q_0 < 10$. Emphasis was made on the ability to control and tune the damping parameter of the junctions. Below, we describe five different ways used for tuning Q_0 in our junctions: together with conventional ways of tuning I_{c0} by applying the magnetic field or changing temperature, we were also able to tune I_{c0} by applying gate voltage, adding a ferromagnetic material into the junction barrier and by tuning C by *in situ* capacitive shunting.

The parameters of the studied junctions are summarized in Table I.

A. Planar superconductor-ferromagnet-superconductor (Nb-CuNi-Nb) junctions

Planar Nb-CuNi-Nb junctions were made by cutting a small Nb/Cu$_{0.47}$Ni$_{0.53}$ bilayer bridge by a focused ion beam (FIB).[25] A sketch of the SFS junction is shown in Fig. 2(a). We made JJ's from two types of Nb/CuNi bilayers with either 70 or 25 nm thick Nb layers. The thickness of the CuNi layer was always 50 nm. In-plane dimensions of the JJ's, presented here, were the same. Details of sample fabrication and characterization can be found elsewhere.[26]

Figures 2(b) and 2(c) show the IVC's at different T for planar SFS junctions made from 70/50 nm and 25/50 nm Nb/CuNi bilayers, respectively. From Fig. 2, it is seen that the IVC's are consistent with the RCSJ model with constant $R \sim 0.25$ Ω. Since $R \ll Z_0 \sim 100$ Ω, shunting by the circuitry

impedance is negligible also at high frequencies.

The critical current depends very strongly on the depth of the FIB cut, especially at the edge of cutting through the top Nb layer, see Fig. 2(a). By varying the depth of the cut, we were able to fabricate JJ's with 3 orders of magnitude difference in I_{c0}.[26] On the contrary, the resistance of junctions remained almost unchanged upon cutting through the top Nb layer, as seen from IVC's in Fig. 2. Since the in-plane geometries of the junctions are the same, C and the thermal con-
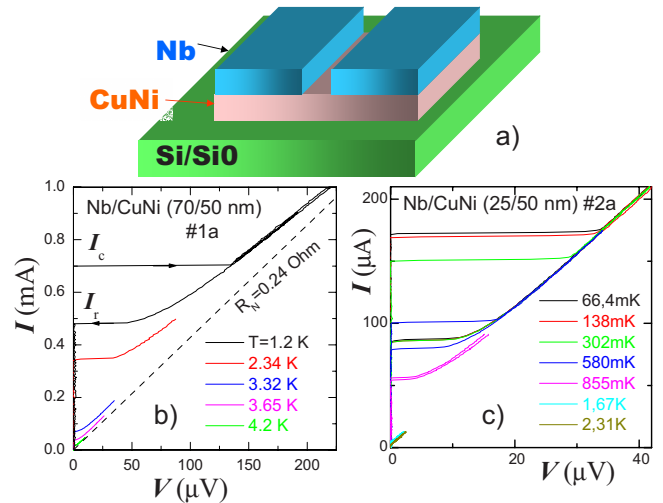

FIG. 2. (Color online) (a) Sketch of the planar Nb-CuNi-Nb junction. The junctions were made by cutting Nb/CuNi bilayers by FIB. Panels (b) and (c) show I-V characteristics at different T for junctions made from 70/50 nm and 25/50 nm thick Nb/CuNi bilayers, respectively. The IVC's of both junctions are RCSJ-like and exhibit hysteresis at low T.
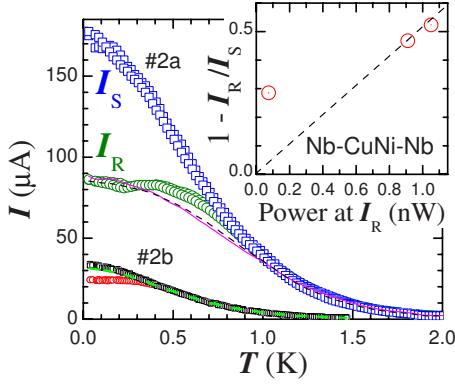
FIG. 3. (Color online) Temperature dependence of the switching and retrapping currents for two SFS junctions made from the same 25/50 nm Nb/CuNi bilayer at $H=0$. It is seen that the hysteresis $I_S > I_R$ exists at low T for both JJ's. Solid and dashed lines represent $I_R(T)$ calculated within the RCSJ and self-heating models, respectively. The inset shows the size of the hysteresis $1 - I_R/I_S$ at the lowest T as a function of the dissipated power at $I = I_R$. Note that the hysteresis is not proportional to the power at retrapping.

ductances of the junctions are also similar. Therefore, by changing the depth of the FIB cut, we could vary in a wide range the Q_0 of the junctions by solely affecting I_{c0} and leaving all other parameters intact.

Figure 3 shows T dependencies of switching and retrapping currents for two JJ's on the same chip. Development of the hysteresis, $I_S > I_R$, with T is seen. The JJ's were fairly uniform, as follows from the clear Fraunhofer modulation of the critical current as a function of magnetic field, shown in Fig. 4(a).

B. Nanosculptured superconductor–normal-metal–superconductor (Nb-Pt-Nb) junctions

Nanoscale SNS junctions were made from Nb-Pt-Nb trilayers[27] by three-dimensional FIB sculpturing. The thicknesses of bottom and top Nb layers were 225 and 350 nm, respectively. The thickness of Pt was 30 nm. A sketch of the junction is shown in the inset of Fig. 5. Nanofabrication was required both for increasing R and decreasing I_{c0} to easily measurable values.

The main panel in Fig. 5 shows a set of IVC's at $T = 3.2$ K for a Nb-Pt-Nb JJ (170×88 nm^2) at different magnetic fields along the long side of the JJ. Strong modulation of the critical current is seen. The IVC's are well described by the RCSJ model with constant $R \simeq 0.6$ $\Omega \ll Z_0$.

Some JJ's were anodized to remove possible shorts caused by redeposition of Nb during FIB etching and to further decrease the junction area. The absence of shorts and the uniformity of junctions was confirmed by clear Fraunhofer modulation of $I_S(H)$, shown in Fig. 6(a). Details of the junction fabrication and characterization were described in Ref. 28 and will be published elsewhere.

C. Superconductor–two-dimensional-electron-gas–superconductor junctions

S-2DEG-S junctions with planar geometry were formed by two Nb electrodes connected via the two-dimensional
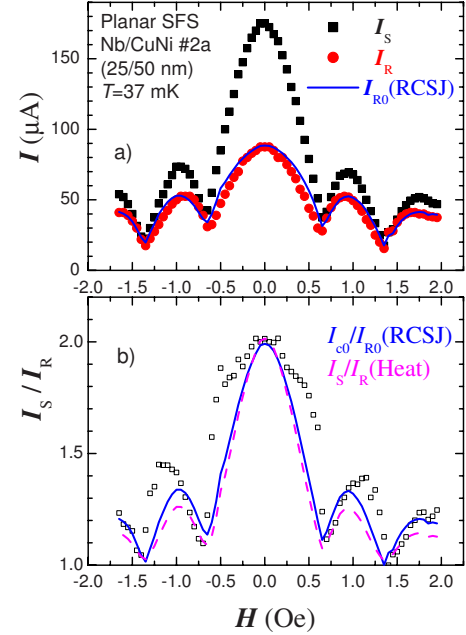

FIG. 4. (Color online) (a) Magnetic field dependence of the switching and retrapping currents for the planar SFS junction 2a at $T = 37$ mK. The solid line is the calculated $I_{R0}(H)$ within the RCSJ model for $Q_0(H=0) = 2.55$. (b) I_S/I_R vs H for the same junction. The solid line is the I_{c0}/I_{R0} within the RCSJ model for $Q_0(H=0) = 2.55$. The dashed line represents I_{c0}/I_R calculated for the case when the hysteresis is caused solely by self-heating (see Sec. IV).

electron gas (2DEG) (InAs).[29] Properties (I_{c0} and R) of the JJ's depend on the width of Nb electrodes (either 10 or 40 μm), the length of the 2DEG (either 400 or 500 nm), and the transparency of the contact between the Nb and the 2DEG.[31] A narrow gate electrode was made on top of the 2DEG, forming a Josephson field-effect transistor.[30] This provides a unique opportunity to tune properties of the JJ's by applying a gate voltage V_g. Details of sample fabrication and characterization can be found elsewhere.[30,31]

Figure 7 shows a set of IVC's at $T = 30$ mK for different V_g. It demonstrates that the critical current is increased at
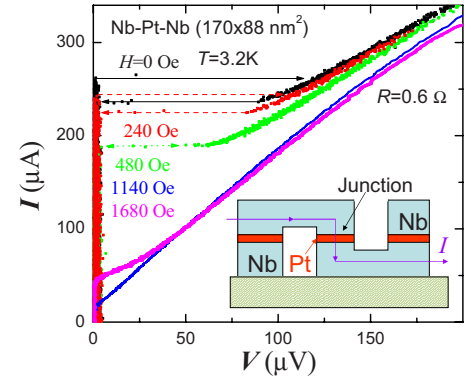

FIG. 5. (Color online) I-V characteristics at different H for a nanosculptured SNS junction at $T = 3.2$ K. The IVC's are RCSJ-like and exhibit hysteresis at small H. Inset shows a sketch of the junction.
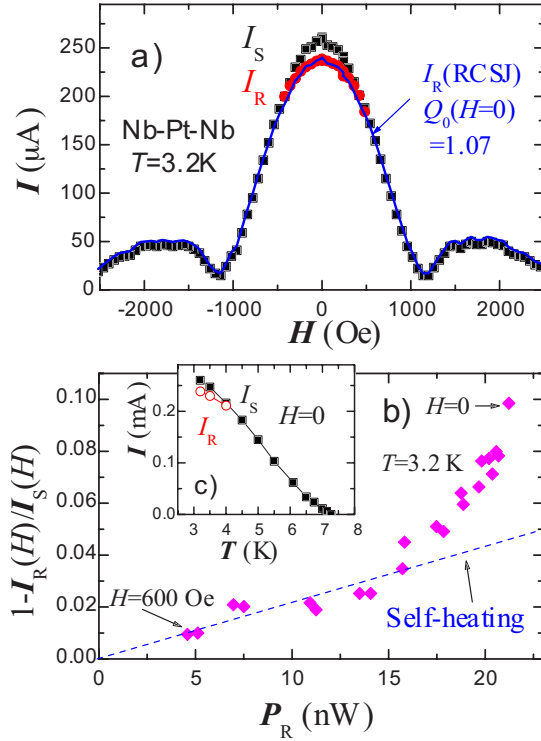
FIG. 6. (Color online) (a) Magnetic field modulation of the switching and retrapping currents at $T=3.2$ K for the same Nb-Pt-Nb junction as in Fig. 5. The solid line represents calculated $I_R(H)$ within the RCSJ model for $Q_0(H=0)=1.07$. (b) The size of hysteresis $1-I_R/I_S$ vs dissipation power at retrapping P_R for the same data JJ. The dashed line represents a characteristic linear dependence typical for self-heating. (c) Temperature dependence of the switching and retrapping currents at $H=0$ for this junction.

positive V_g and strongly suppressed at small negative V_g. Note that the resistance of the junction starts to increase at substantially larger negative $V_g \lesssim -1$ V, at which the critical current is already strongly suppressed. Therefore, the IVC's at $V_g > -1$ V are reasonably well described by the RCSJ model with a constant R.

The majority of switching current measurements were performed on the junction 2b with a wide (40 μm) and short (400 nm) 2DEG and good transparency of the Nb/2DEG in-
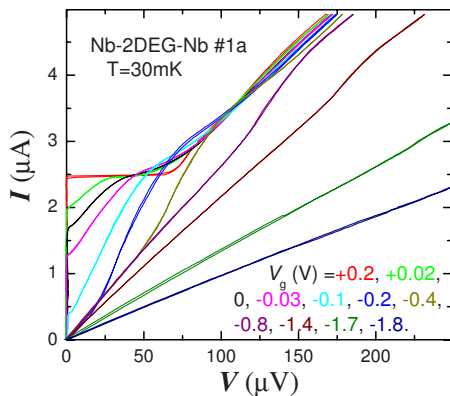

FIG. 7. (Color online) The IVC's of a S-2DEG-S junction for different gate voltages at $T=30$ mK.
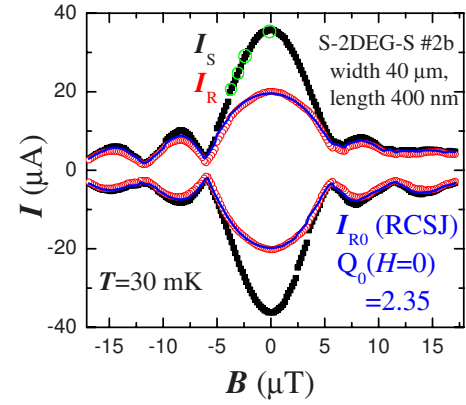

FIG. 8. (Color online) Magnetic field modulation of switching and retrapping currents for the S-2DEG-S junction 2b at $T=30$ mK. The solid line represents a simulation within the RCSJ model for $Q_0(H=0)=2.35$.

terface. For 40 μm wide junctions, shunting by high frequency impedance was insignificant because of the small junction resistance $R \simeq 7.5-10$ Ω. Junctions with narrower 2DEG (10 μm) had proportionally smaller I_{c0} and larger $R \sim 30-40$ Ω. All JJ's studied here had a uniform critical current distribution, as judged from periodic Fraunhofer modulations $I_S(H)$, see Fig. 8.

Figure 9 shows the T dependencies of I_S and I_R for the same JJ at two magnetic fields, marked by circles in Fig. 8. The T dependence of I_S and I_R for S-2DEG-S JJ's is similar to that of planar SFS JJ's, see Fig. 3. In both cases, the I_R is T independent in a wide T range.

D. Bi-2212 intrinsic Josephson junctions

Intrinsic Josephson junctions (IJJ's) are naturally formed between adjacent Cu-O layers in strongly anisotropic HTSC single crystals.[32] IJJ's behave as SIS-type junctions[33,34] with high Q_0, in spite of the d-wave symmetry of the order pa-
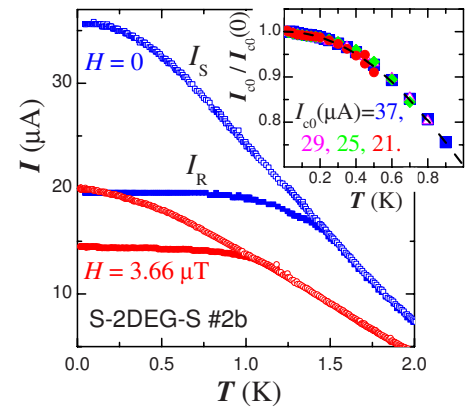

FIG. 9. (Color online) T dependence of the switching and retrapping currents for the S-2DEG-S junction 2b at magnetic fields marked by two of the circles in Fig. 8. The inset shows T dependencies of normalized fluctuation-free critical currents $I_{c0}(T)/I_{c0}(T=0)$ at four H marked in Fig. 8.
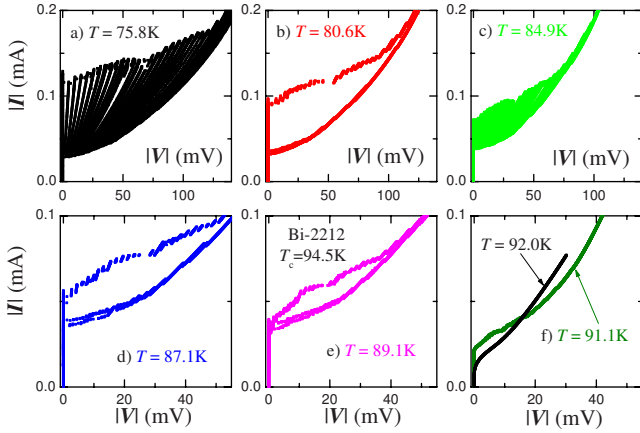
FIG. 10. (Color online) Four-probe I-V characteristics of a Bi-2212 mesa at different temperatures. It is seen that the multibranch structure and the hysteresis persist up to ~3 K below T_c.

rameter in HTSC. This was confirmed by observation of geometric Fiske resonances[35,36] and energy level resolution in the MQT experiments on Bi-2212 IJJ[37] and $YBa_2Cu_3O_{7-\delta}$ biepitaxial c-axis (IJJ-like) JJ's.[20]

IJJ's were made by micro- and/or nanopatterning of small mesa structure on top of Bi-2212 single crystals. Here, we present data for an optimally doped Bi-2212 single crystal with $T_c \simeq 94.5$ K. Mesas were cut in two parts by FIB to allow true four-probe measurements. Details of mesa fabrication can be found elsewhere.[38] Properties of our IJJ's were described in detail before.[33,34] Figure 10 shows IVC's at different T for a Bi-2212 mesa. IVC's of IJJ's are nonlinear and exhibit strong hysteresis below T_c. However, at elevated temperatures, 70 K$< T < T_c$, the IVC's are almost linear in a small voltage range.[2,33] Each mesa contains several stacked IJJ's. Therefore, IVC's exhibit a multibranch structure due to one-by-one switching of stacked IJJ's from S to R state.

Figure 11 shows the T dependence of the most probable switching current I_{Smax}, the retrapping current I_R, and the fluctuation-free critical current I_{c0} for a single IJJ from the same Bi-2212 sample as in Fig. 10.[39] The I_{c0} was obtained from the analysis of switching statistics.[38] The $I_{c0}(T)$ follows the Ambeokar-Baratoff dependence typical for conventional
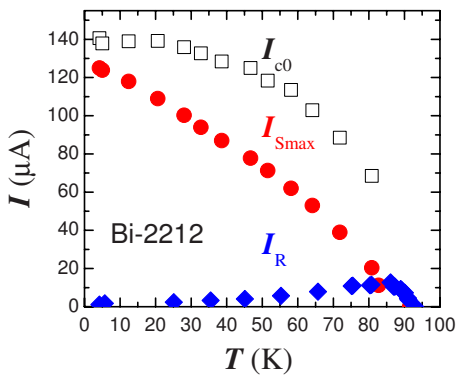

FIG. 11. (Color online) Temperature dependence of the most probable switching I_{Smax}, retrapping I_R and fluctuation-free critical I_{c0} currents for the same Bi-2212 IJJ.

SIS JJ's.[38] The I_R is T independent at low T and increases with T up to ~85 K. Such behavior is also typical for conventional SIS JJ's and is attributed to strong T dependence of the low bias quasiparticle resistance, which determines the effective dissipation for the retrapping process.[40]

IV. ORIGIN OF HYSTERESIS

Figures 2–11 show that the IVC's of all the four types of JJ's studied here exhibit a hysteresis at low T.

For the case of Bi-2212 IJJ's, the hysteresis can be unambiguously attributed to a large capacitance caused by atomic scale separation between electrodes. From measurements of Fiske step voltages,[35] the specific capacitance of our IJJ's was estimated as $C \sim 68.5$ fF$/\mu m^2$. Substituting typical parameters of IJJ's,[34] the critical current density $J_c(4.2$ K$) \simeq 10^3$ A/cm^2, the large bias c-axis tunnel resistivity $\rho_c \simeq 30$ Ω cm, and the stacking periodicity $s \simeq 1.5$ nm, we obtain $Q_0(4.2$ K$) \simeq 20$. This value will become up to 2 orders of magnitude larger if we use the low bias quasiparticle resistivity at T=4.2 K instead of ρ_c. In any case, IJJ's are strongly underdamped, $Q_0 \gg 1$, at $T \ll T_c$ and also remain underdamped in practically the whole T range $T < T_c$, as seen from Fig. 11. It has been demonstrated that the hysteresis I_S/I_R in Bi-2212 IJJ's agrees well with the calculated Q_0 using the specific capacitance of IJJ's.[38]

On the other hand, explanation of the hysteresis in SNS-type JJ's is less straightforward. Typically, SNS JJ's are strongly overdamped, $Q_0 \ll 1$, and the hysteresis is caused by either self-heating,[41] nonequilibrium effects,[42] or frequency dependent damping,[9] rather than the junction capacitance.

According to the RCSJ model, the hysteresis is related to damping and appears in underdamped JJ's with $Q_0 > 0.84$. If the hysteresis were due to finite junction capacitance, then magnetic field modulation of $I_{R0}(H)$ should be a unique function of $I_{c0}(H)$, given by Eqs. (9) and (10) with field dependent $Q_0(H) = Q_0(H=0)[I_{c0}(H)/I_{c0}(H=0)]^{1/2}$, as follows from Eq. (1). The corresponding $I_{R0}(H)$ curves calculated within the RCSJ model are shown by solid lines in Figs. 4, 6(a), and 8. In all cases, the agreement with the experimental data is remarkable, considering that there is only one fitting parameter $Q_0(H=0)$ for each curve (indicated in the figures). However, as it will be shown below, such a fit can be misleading because self-heating can produce exactly the same result, as shown by the dashed line in Fig. 4(b).

A. Self-heating

It is known that self-heating can cause hysteresis in superconducting weak links with negligible C.[41] In this case, the "retrapping" current simply represents I_S at the elevated temperature due to power dissipation at the resistive branch of the IVC:

$$I_R = I_S[T_0 + \Delta T(I_R)] \simeq I_S(T_0) + \frac{dI_S}{dT}\Delta T(I_R), \quad (16)$$

$$\Delta T(I_R) = P_R R_{th} \simeq R R_{th} I_R^2, \qquad (17)$$

where R_{th} is the thermal resistance of the junction and P_R is the power dissipation at I_R. One can easily solve the system of Eqs. (16) and (17):

$$I_R \simeq \frac{\sqrt{1 + 4\alpha I_S^2} - 1}{2\alpha I_S}, \qquad (18)$$

$$1 - \frac{I_R}{I_S} \simeq \frac{\alpha}{R} P_R, \qquad (19)$$

where $\alpha = -(dI_S/dT)RR_{th}/I_S(T_0)$. This solution is valid for small self-heating, except for the case of linear $I_S(T)$ and T-independent R_{th}, when it is correct for arbitrary self-heating.

The dashed line in Fig. 4(b) shows a fit to experimental $I_R(H)$ within the self-heating model, Eq. (18). The solid line in the same figure represents the fit within the RCSJ model, Eqs. (1) and (10). $I_R(H)$ for both self-heating and RCSJ models were obtained using a single fitting parameter, R_{th} and $Q_0(H=0)$, respectively, which are unambiguously determined from hysteresis I_S/I_R at $H=0$. Obviously, the self-heating and RCSJ models provide equally good and almost indistinguishable fits to experimental $I_R(H)$. Similarly, T dependencies of I_R within the two scenarios are practically the same, as seen from comparison of dashed and solid lines in Fig. 3.

Therefore, discrimination between capacitive and self-heating origins of the hysteresis cannot be made from just analyzing T or H dependencies of I_S and I_R but requires additional experimental data. One way to check the origin of hysteresis is to study P_R dependence of I_R and analyze the consistency with Eq. (19). This has to be done at constant base T for samples with the same R_{th} to avoid the unknown T dependence of R_{th}. The easiest way to perform such a test is to analyze the magnetic field dependence at constant T, because small field affects only I_S, I_R, and P_R, but not R_{th}, or the shape of $I_{c0}(T)$ (as seen from the inset of Fig. 9). According to Eq. (19), the size of the hysteresis, caused by self-heating, must be proportional to P_R, at least at small P_R. On the other hand, from Eqs. (1) and (9), the capacitive hysteresis, modulated by magnetic field, changes as $1 - I_R(H)/I_S(H) \simeq 1 - [4\pi/Q_0(H=0)]\sqrt{P_R(0)/P_R(H)}$.

Figure 6(b) shows the experimental magnetic field dependence of the hysteresis $1 - I_R(H)/I_S(H)$ on P_R at constant base $T_0=3.2$ K for the SNS junction. Here, $I_R(H)$ and $I_S(H)$ were taken from Fig. 6(a), and $P_R(H)$ was obtained from simultaneously measured IVC's, shown in Fig. 5. It is seen that the hysteresis vanishes linearly at small P_R, consistent with the self-heating scenario and inconsistent with the capacitive scenario of the hysteresis. At larger P_R, the hysteresis becomes larger than predicted by the self-heating model (the dashed line). Deviation from the linearity at large self-heating may occur due to T dependence of I_S and R_{th}. The former tends to increase the hysteresis in case of larger dI_S/dT at higher T, and the latter–to decrease the hysteresis due to smaller R_{th} at higher T. However, none of those corrections can explain such a large deviation. This becomes clear from the analysis of T dependencies of I_S and I_R at $H=0$, shown in Fig. 6(c). From Fig. 6(c), it is seen that ΔT at $T_0=3.2$ K cannot exceed 0.4 K. Thus, even at the largest P_R in Fig. 6(b), the self-heating is small, $\Delta T/T_0 < 0.13$, and second-order corrections to linear P_R dependence within the self-heating scenario are negligible. The strong deviation from linearity probably indicates the existence of an additional hysteresis mechanism at large bias. However, as will be discussed below, the capacitance of this junction is clearly too small to cause extra hysteresis. On the other hand, the additional hysteresis may be caused by nonequilibrium effects[42] in this SNS JJ with high critical current density.

A clue to the origin of hysteresis can also be obtained from comparison of IVC's of JJ's with identical geometry but different I_S. As described in the previous section, a minor variation of the FIB-cut depth in the planar SFS JJ's changes I_{c0} by several orders of magnitude without affecting other characteristics of JJ's (C, R, and R_{th}), see Figs. 2 and 3. The inset of Fig. 3 shows the values $1 - I_R/I_S$ at $T \simeq 30$ mK for three SFS JJ's with similar geometry on the same chip. The dashed line shows the linear P_R dependence, expected within the self-heating scenario. Provided the hysteresis in JJ's with larger I_{c0} is caused by self-heating, and R_{th} of all three JJ's are the same, there should be no hysteresis due to self-heating for the JJ with the smallest I_{c0}. This is indicated by the green (lower) dashed line in the main panel of Fig. 3, which represents the self-heating $I_R(T)$ for the JJ with small I_S, calculated from Eq. (18) using the parameter α obtained from the fit $I_R(T)$ for the JJ with larger I_S, shown by the black (upper) dashed line in Fig. 3. Thus, self-heating does not satisfactorily explain the hysteresis in SFS junctions, although it is probably responsible for a considerable part of the hysteresis in JJ's with larger I_S.

For Bi-2212 IJJ's, self-heating was measured directly[43] for the same mesa. The R_{th} of the mesa ranged from ~ 70 K/mW at $T=4.2$ K to ~ 10 K/mW at 80 K. Since the dissipated power at $I < I_S$ at the first branch in the IVC never exceeded a few microwatts, self-heating can be excluded as the origin of hysteresis in IJJ's.

B. Capacitance

In order to understand whether the finite junction capacitance may contribute to the hysteresis, we first calculate C that are required for reaching $Q_0=1$: $C[Q_0(H=0)=1] \sim 35$ pF for SFS 2a (Fig. 4), ~ 4 pF for SNS (Fig. 6), and ~ 0.2 pF for S-2DEG-S 2b (Fig. 8) JJ's, respectively. These must be compared with the expected geometrical C of the JJ's.

The overlap capacitance of the SNS junction, Fig. 6, is small, approximately a few femtofarads, due to small area of the JJ ($\sim 0.015 \ \mu m^2$). The stray capacitance was estimated to be of the same order of magnitude. Therefore, the total C of this junction is insufficient for observation of the hysteresis within the simple RCSJ model. Therefore, as discussed in connection with Fig. 6(b), the hysteresis in this JJ must be attributed to self-heating and, perhaps, nonequilibrium phenomena at high bias.

The total (stray) capacitance of wide S-2DEG-S JJ's with the gate electrode is estimated to be $\sim 0.1 - 0.2$ pF. This C
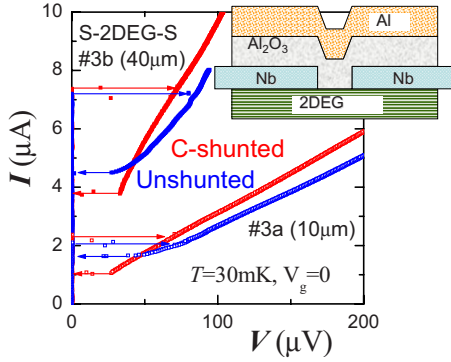
FIG. 12. (Color online) IVC's of two S-2DEG-S junctions on the same chip at $T=30$ mK, $H=0$, before and after *in situ* C shunting. Inset shows a sketch of the C-shunted junction.

can cause a substantial hysteresis in junction 2b with large I_{c0} and may be just sufficient for a tiny hysteresis in the other junctions with smaller I_{c0}. This conclusion is also supported by observation of underdamped phase dynamics in those junctions, as will be discussed below.

We argued above that the hysteresis in SFS JJ's cannot be caused solely by self-heating. However, how could the huge $C \sim 35$ pF appear in those planar JJ's with the stray capacitance in the range of few femtofarads? To understand this, we should consider the specific junction geometry, shown in Fig. 2(a). The JJ's are made of Nb/CuNi bilayers. The CuNi layer may act as a ground plane for the JJ and may create the large overlap capacitance, provided there is a certain barrier for electron transport between the layers. The transparency of Nb/Cu interfaces, made in the same setup, was previously estimated to be ~0.4.[44–46] The interface transparency between Nb and CuNi is expected to be even smaller due to appearance of excess interface resistance between normal metals and spin-polarized ferromagnets.[47] For typical values of the overlap capacitance $C \sim 20$–40 fF/μm^2, the required $C \sim 35$ pF can originate from the bilayer within just ~30–40 μm radius from the JJ. An unambiguous confirmation of the presence of the large C in our SFS JJ's follows also from observation of the underdamped phase dynamics, as reported below (Fig. 16).

C. *In situ* capacitive shunting

To clarify the origin of hysteresis, we fabricated an *in situ* shunt capacitor, consisting of 300 μm wide Al$_2$O$_3$/Al double layer deposited right on top of S-2DEG-S JJ's. The sketch of the C-shunted junction is shown in Fig. 12. The IVC's for two JJ's from the same chip before and after C shunting are shown in Fig. 12. The length of 2DEG in those junctions was 500 nm, which results in considerably smaller I_{c0} than for the JJ 2b with 400 nm long 2DEG, see Table I. It is seen that the hysteresis for both junctions increased considerably, while R was little affected by C shunting.[48] The total capacitance of the shunt was ~5 pF, much larger than the initial capacitance of unshunted junctions $C \sim 0.1$–0.2 pF.

It should be emphasized that introduction of the C shunt improves thermal conductance from the junctions. Indeed, since the sample was placed in vacuum, the C-shunt double
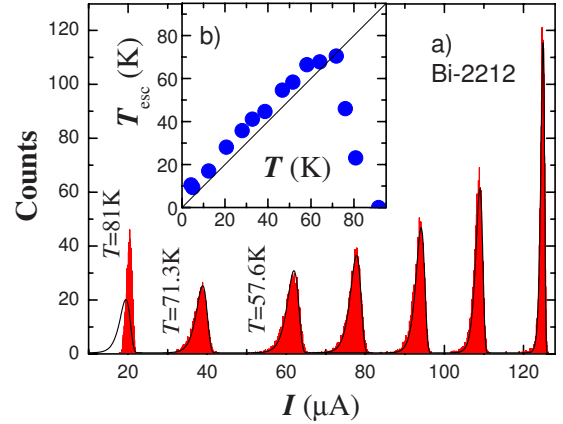

FIG. 13. (Color online) (a) Switching histograms of a single IJJ at different T. The solid lines represent theoretical results for thermal activation at a given T. Note that the experimental histograms initially become wider with increasing T but suddenly become narrower and change the shape at T^* between 71 and 81 K. (b) The effective escape temperature vs T extracted from fitting the switching histograms to the TA theory. The solid line represents the prediction of conventional TA theory, $T_{esc}=T$. A sudden collapse of T_{esc} is seen at $T^* \simeq 75$ K.

layer on top of the 2DEG acts as the top heat spreading layer,[49,50] creating an additional heat sinking channel. Thus, the self-heating hysteresis must decrease in the C-shunted JJ. Therefore, increase of the hysteresis in C-shunted JJ's unambiguously indicates that the hysteresis in those JJ's is indeed caused by the junction capacitance, rather than self-heating.

To summarize this section, identification of the mechanism of hysteresis is quite intricate, in particular, due to the frustratingly similar behavior of $I_R(T,H)$ within self-heating and RCSJ models. Table I presents values of Q_0 for the studied junctions. In all cases, these values were obtained from a self-consistent analysis of a complete set of data for the specific sample, including (i) P_R dependence of the hysteresis, see Figs. 3 and 6, (ii) estimation of the junction capacitance from quantum fluctuations, as shown in Fig. 15(b), and (iii) observation of the underdamped phase dynamics in the collapse state, see Figs. 13–16, 18, and 20.

Thus, we arrive at the following conclusions about the origin of hysteresis in our JJ's: For IJJ's, the hysteresis is caused solely by the junction capacitance. The C-shunted S-2DEG-S JJ's are underdamped, with predominantly capacitive hysteresis. For most SNS-type junctions, the hysteresis is considerably affected by self-heating. However, planar SFS and S-2DEG-S junctions 2b with short (400 nm) 2DEG are underdamped, $Q_0 \gtrsim 1$, at low T. Therefore, a substantial part of hysteresis in those junctions has a capacitive origin.

V. COLLAPSE OF SWITCHING HISTOGRAMS

Measurements of switching and retrapping current statistics were made in a carefully shielded dilution refrigerator (sample in vacuum) in a shielded room environment. Measurements in the temperature range 1.2–100 K were made in a He^4 cryostat (sample in liquid or gas). Switching and re-
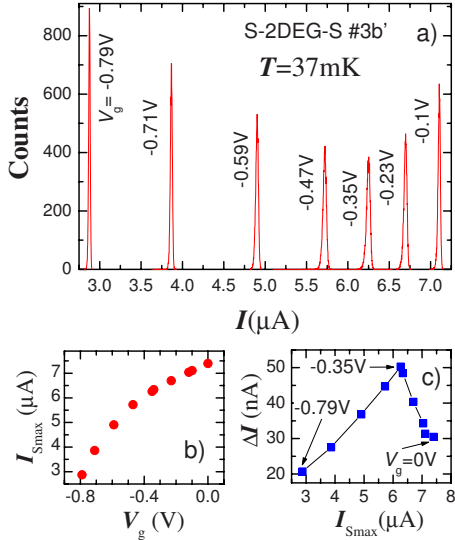
FIG. 14. (Color online) (a) Switching histograms of S-2DEG-S 3b′ at $T=37$ mK for different gate voltages V_g. It is seen that the height (inversely proportional to the width) of the histograms first decreases but then starts to increase with increasing negative V_g. (b) Dependence of the most probable switching current I_{Smax} on the gate voltage. (c) The width of the histograms ΔI vs I_{Smax}. A sudden collapse of ΔI occurs at $V_g < -0.35$ V.

trapping currents were measured using a standard sample-and-hold technique. All histograms were made for 10 240 switching events.

A. Collapse in Bi-2212 intrinsic Josephson junctions

A sporadic switching of simultaneously biased stacked IJJ's in the Bi-2212 mesa results in rather chaotic switching between quasiparticle branches in the IVC, see Fig. 10. This makes the analysis of switching statistics quite complicated. In addition, strong electromagnetic coupling of atomic scale stacked IJJ's in the mesa leads to the appearance of meta-stable fluxon states[51,54] and results in multiple valued critical current.[51,53] It has been reported that switching histograms of IJJ's can be very broad and contain multiple maxima,[51–53] consistent with frustration caused by the presence of meta-stable states in long, strongly coupled stacked JJ's.[51,53]

In order to avoid the metastable states, we studied switching statistics of a single IJJ.[38,39] In the studied mesa, one of the junctions occasionally had slightly smaller I_{c0} (by ~20%) than the rest of the IJJ's. Thus, we were able to achieve stable switching of this single IJJ, while the rest of the IJJ's remained in the S state.[38]

Figure 13 shows switching histograms for the single IJJ at different T. The black solid lines represent simulated histograms for conventional TA escape, Eqs. (2) and (13), at given T and for corresponding junction parameters and experimental sweeping rates. Detailed analysis of the switching histograms can be found elsewhere.[38] The switching histograms are perfectly described by the TA theory up to $T^* \sim 75$ K. However, at higher T, the histograms suddenly become narrower. This is clearly seen from Fig. 13(b) which represents
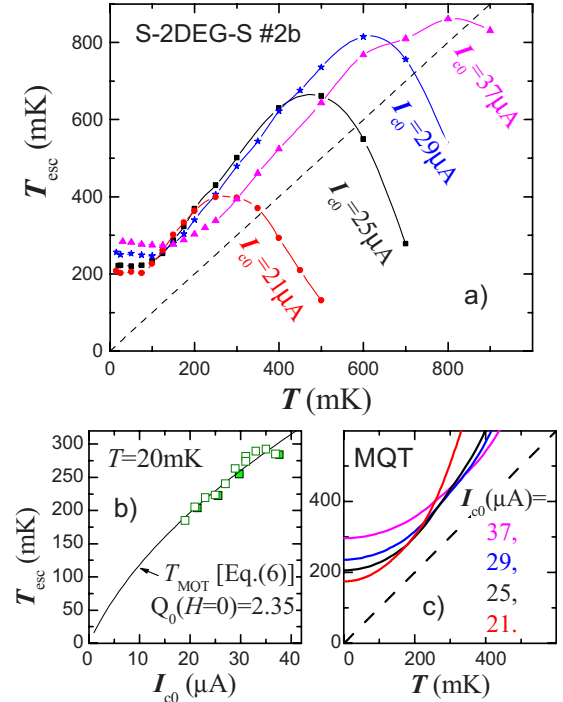

FIG. 15. (Color online) (a) Escape temperature vs T for the S-2DEG-S JJ 2b at four magnetic fields (marked by circles in Fig. 8). Three T regions can be distinguished: the MQT at low T, the TA at intermediate T, and the collapse region at $T > T^*$. (b) T_{esc} in the MQT state at $T=20$ mK as a function of the fluctuation free I_{c0}, suppressed by applying magnetic field. Solid line represents the fit to Eq. (6) for $Q_0(H=0)=2.35$. (c) Results of MQT simulations, Eq. (5), for the experimental conditions in panel (a).

the effective escape temperature T_{esc} obtained from the fit of experimental escape rate by the TA expression, Eq. (2), with $T=T_{esc}$ being the fitting parameter. T_{esc} represents the strength (amplitude) of thermal fluctuations in the JJ and for conventional TA, $T_{esc}=T$, as shown by the solid line in Fig. 13(b). A sudden collapse of T_{esc} at $T^* \simeq 75$ K is clearly seen from Fig. 13(b). We also note that the histograms become progressively more symmetric at $T > T^*$.

B. Collapse in superconductor–two-dimensional-electron-gas–superconductor junctions

S-2DEG-S junctions provide a unique opportunity to tune I_{c0}, E_{J0}, and Q_0 by applying the gate voltage V_g, see Fig. 7. Figure 14(a) shows switching current histograms at $T=37$ mK for the S-2DEG-S 3b′ (identical to 3b) at different V_g. Panel (b) shows that the most probable switching current I_{Smax} decreases monotonously with increasing negative V_g. Panel (c) shows the width at half-height ΔI versus I_{Smax}. It is seen that initially, histograms are getting wider with increasing negative V_g due to the increase of TA with decreasing E_{J0}/T. However, at $V_g < -0.35$ V, a sudden change occurs and ΔI starts to rapidly collapse.

Figure 15(a) shows T_{esc} vs T for the S-2DEG-S 2b at $H=0$, 2.32, 3.05, and 3.66 μT (marked in Fig. 8). In all cases, we can distinguish three T regions.
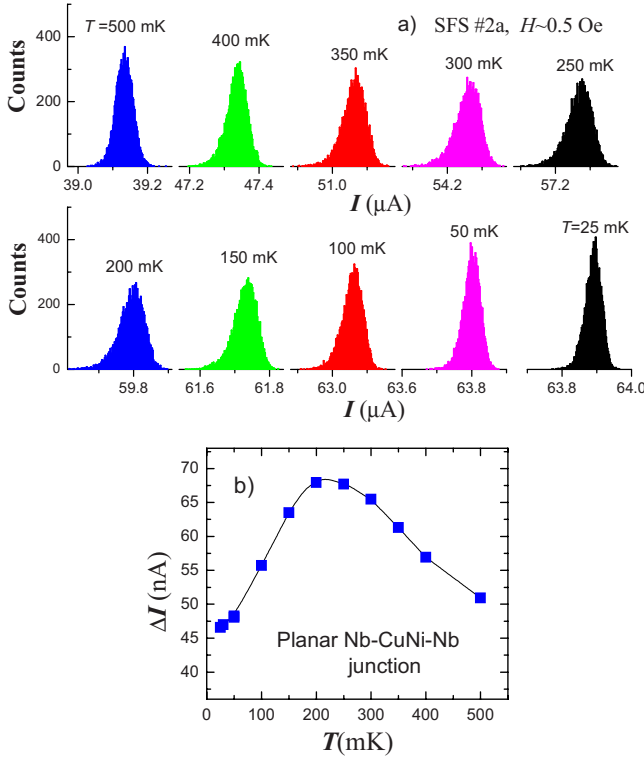
FIG. 16. (Color online) (a) Switching histograms of the planar SFS junction 2a at different T. The histograms become wider with increasing T up to $T=200$ mK (lower row) but then the width starts to shrink at $T \gtrsim 250$ mK (upper row). (b) The width of histograms ΔI vs T. The $\Delta I(T)$ follows the TA behavior up to $T^* = 200$ mK but collapses at higher T.

(i) The MQT regime. At low T, T_{esc} is independent of T. Both the TA-MQT crossover temperature, at which saturation of $T_{esc}(T)$ occurs with decreasing T, and the value of $T_{esc}(T \to 0)$ decrease with H, which leaves no doubts that we observe the MQT state.[7,9–11] Figure 15(b) shows the dependence of the T_{esc} at $T=20$ mK as a function of $I_{c0}(H)$. I_{c0} for each H was extrapolated from the switching histograms. The inset of Fig. 9 demonstrates that $I_{c0}(T)/I_{c0}(T \to 0)$ for different H collapse into one curve, confirming the accuracy of determination of $I_{c0}(T,H)$. The solid line in Fig. 15(b) shows the fit to the TA-MQT crossover temperature, Eq. (6), taking $Q_0(H=0)=2.35$, following from the value of hysteresis in the IVC's, see Fig. 8. Obviously, the MQT calculations are consistent with the previous conclusion that this JJ is underdamped at low T and that the hysteresis in this JJ is predominantly caused by the junction capacitance.

We tried to perform quantum level spectroscopy[20] in the MQT state for this JJ, but we could not observe any interlevel transitions. This implies that the level width $\sim \hbar/(RC)$ is of the order of level spacing $\hbar \omega_p$, which, in turn, is caused by a relatively low Q_0 for this JJ [recall that Q_0 decreases with H according to Eq. (1)]. A similar evidence for the MQT, i.e., saturation of T_{esc} at $T \to 0$, was observed even for more damped JJ's SFS 2a, see Fig. 16(b), and unshunted S-2DEG-S 3b, see Fig. 18(b), with $Q_0 \lesssim 1$, see Table I. Therefore, our data confirm the theoretical prediction[7,8] that
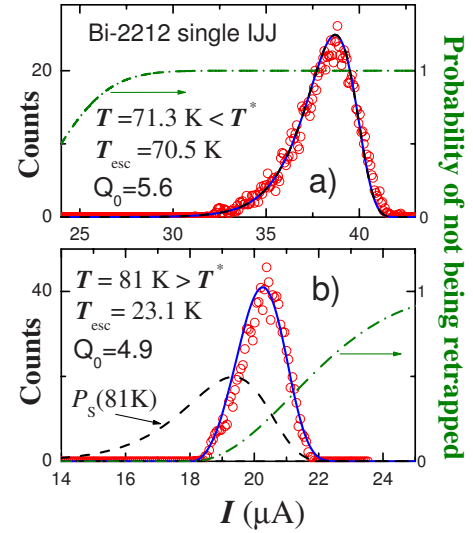

FIG. 17. (Color online) Switching histograms of a single IJJ (a) below and (b) above the collapse temperature $T^* \simeq 75$ K. Symbols represent experimental data: dashed lines, TA probability density of $S \to R$ switching; dashed-dotted lines, probabilities of not being retrapped $\mathbb{P}_{nR}$, Eq. (15). Solid lines show the conditional probability density P_{SR} of switching without being retrapped. It is seen that close to the collapse temperature, the retrapping process becomes significant and effectively "cuts off" thermal activation at small bias. Note that both the width and the shape of the histograms change at T^*. Data from Ref. 2.

the MQT occurs even in the absence of well defined quantum levels in slightly underdamped and overdamped JJ's, $Q_0 \lesssim 1$. Both the absolute value and the characteristic parabolic shape of $T_{esc}(T)$ in the MQT state are in good agreement with theoretical predictions, as shown in Fig. 15(c). The solid lines in Fig. 15(c) show simulated T_{esc} vs T in the MQT state, calculated from Eq. (5) using the experimental conditions for the data in Fig. 15(a). It is seen that both the absolute value and the shape of simulated $T_{esc}(T)$ agree with the experimental data.

(ii) Thermal activation regime. At intermediate T, ΔI increases in agreement with TA calculations, $T_{esc}=T$ shown by dashed lines in Fig. 15(a). Slightly larger inclination of the

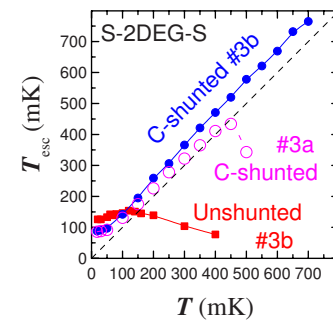FIG. 18. (Color online) Escape temperature vs T for the S-2DEG-S junctions on chip 3 before and after *in situ* C shunting. It is seen that the conventional TA behavior, $T_{esc}=T$, is restored upon increasing Q_0 after C shunting.
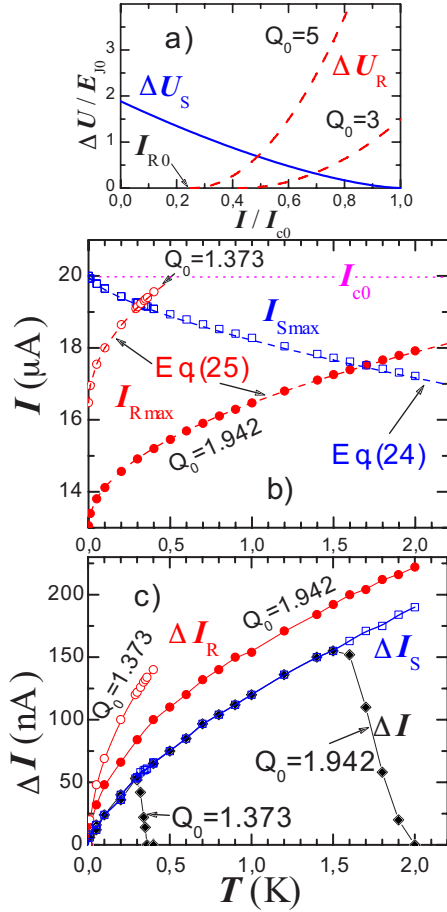
FIG. 19. (Color online) (a) Escape and retrapping barrier heights as a function of bias current for $Q_0=3$ and 5. (b) Numerical simulations of the T dependencies of the most probable switching I_{Smax} and retrapping I_{Rmax} currents for two values of Q_0. Simulations were made for T-independent $I_{c0}=20$ μA (dotted line) and parameters typical for the S-2DEG-S 2b junction. (c) The simulated width of switching ΔI_S and retrapping ΔI_R histograms disregarding the mutual influence of switching and retrapping processes. ΔI is the resulting width of histograms taking into account switching and retrapping. From (b) and (c), it is seen that the collapse of ΔI occurs at the condition $I_{Smax} \simeq I_{Rmax}$.

experimental $T_{esc}(T)$ may be due to nonsinusoidal CPR in this SNS-type JJ.[24]

(iii) Collapse of thermal activation. At higher T, the width of histograms starts to rapidly collapse, leading to a downturn of $T_{esc}(T)$. The magnetic field dependence from Fig. 15(a) reveals that the collapse temperature T^* decreases quite rapidly with I_{c0}, i.e., the collapse occurs at lower T in junctions with smaller Q_0.

C. Collapse in planar superconductor-ferromagnet-superconductor junctions

Figure 16 shows switching current statistics at different T for the planar Nb-CuNi-Nb junction 2a at $H \simeq 0.5$ Oe. The scales of both axes were kept constant for all histograms to facilitate direct comparison of the histograms at different T. It is seen that the collapse of TA occurs at $T^* \simeq 200$ mK.
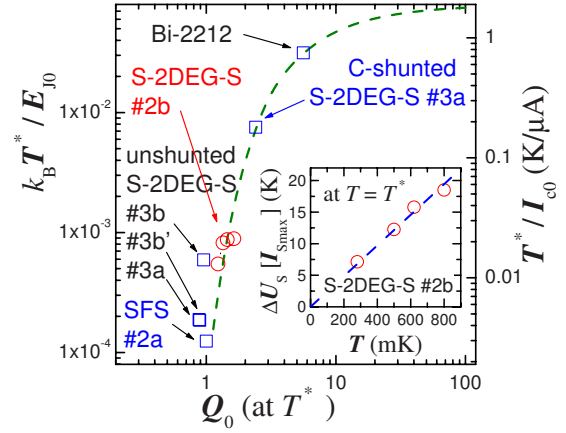

FIG. 20. (Color online) The log-log plot of the normalized collapse temperature vs the quality factor: dashed line represents numerical solution of Eq. (26) and symbols represent experimental data for different JJ's. Inset shows the height of the escape barrier at the most probable switching current as a function of T (at $T=T^*$): symbols represent experimental data for S-2DEG-S 2b from Fig. 15(a) and the dashed line corresponds to Eq. (23).

D. Shape of switching histograms

Figure 17 shows switching histograms of the same single IJJ as in Fig. 13 just before and after the collapse. It demonstrates that not only the width but also the shape of the histogram changes upon the collapse. At $T<T^*$, the histograms have the characteristic asymmetric shape, perfectly consistent with the TA theory,[38] as shown by the black dashed line (coincides with the blue solid line) in Fig. 17(a). However, at $T>T^*$, histograms become narrower and lose the characteristic asymmetric shape, as seen from Fig. 17(b). Such a tendency was observed for all JJ's, as can be seen from Figs. 13, 14, and 16. In Sec. VI below, we will argue that the transformation of the histogram shape at $T>T^*$ is caused by the interference of switching and retrapping processes.

E. Effect of C shunting

Figure 18 shows T_{esc} vs T obtained from switching current statistics, for the same S-2DEG-S JJ's as in Fig. 12, before and after capacitive shunting. Apparently, C shunting qualitatively changed the phase dynamics of the junctions, even though it had a minor effect on I_{c0} and R. However, C shunting strongly affected the quality factor of the JJ's. From Fig. 18, it is seen that the switching statistics of the underdamped C-shunted JJ 3b is well described by the TA theory, for which $T_{esc}=T$. On the contrary, for the unshunted junction, which is just at the edge of being overdamped, $Q_0 \simeq 1$, the T_{esc} decreases with increasing T almost in the whole T range.

F. Failure of the thermal activation theory in moderately damped junctions

The observed collapse cannot be caused by frequency dependent damping due to shunting by circuitry impedance.[9] Indeed, we observed the collapse in planar SFS junctions with $R<1$ Ω, for which such shunting plays no role. Neither

can it be due to T dependence of the TA prefactor a_t in Eq. (4), because damping changes only gradually through T^* and enters only into the (logarithmic) prefactor a_t of the TA escape rate, Eq. (2). Gradual variations of $a_t(T)$ do not cause any dramatic variation of the TA escape rate. Moreover, in all calculations presented here, we did take into account the $Q(T)$ dependence of the TA prefactor a_t, so that T_{esc} must, by definition, be equivalent to T for the conventional TA and the drastic drop in T_{esc} at $T > T^*$ cannot be explained within a simple TA scenario. Therefore, the observed collapse of switching current fluctuations with increasing T represents a dramatic failure of the classical TA theory, which was supposed to be valid even for overdamped JJ's.[4,7]

VI. DISCUSSION

From Figs. 13–16 it is clear that these very different JJ's exhibit the same paradoxical collapse of switching current fluctuations with increasing T. A very similar collapse was observed also in moderately damped SIS type Al-AlO$_x$-Al (Ref. 1) and Nb-AlO$_x$-Nb (Ref. 3) junctions and superconducting quantum interference devices (SQUID's). Therefore, the collapse of TA must be a general property of all moderately damped JJ's.

The dramatic effect of C shunting on the collapse T^* clearly shows that damping has a crucial significance for the observed phenomenon. From the experimental data presented above, it is also clear that T^* decreases with increasing damping and that for overdamped junctions $T^* \to 0$, see the curve for unshunted JJ 3b in Fig. 18. The data also show that the T^* is close to the temperature at which the hysteresis in IVC's vanishes, compare Figs. 3, 16, 9, 15(a), 11, and 13, which implies that retrapping processes may become important in the vicinity of the collapse state.

A. Influence of retrapping on the switching statistics of moderately damped junctions

The paradoxical collapse of thermal fluctuations of I_S and the corresponding failure of the conventional TA theory in moderately damped JJ's can be explained by the influence of retrapping processes on the switching current statistics.[1–3] Indeed, in moderately damped junctions, I_{c0} and I_{R0} are close to each other. As discussed in Sec. II, increasing T tends to decrease I_S and increase I_R. Therefore, at sufficiently high T, both switching and retrapping events may become possible at the same bias. If so, the criterion for measuring the switching event has to be reformulated: The probability of switching from the S to the R state is a conditional probability of switching and not being retrapped back, during the time of experiment,

$$P_{SR}(I) = P_S(I)\mathbb{P}_{nR}(I). \qquad (20)$$

Here, P_{SR} is the probability density of measuring the switching event, P_S is the probability density of switching, Eq. (13), and $\mathbb{P}_{nR}$ is the probability of not being retrapped, Eq. (15).

Dashed-dotted lines in Figs. 17(a) and 17(b) show $\mathbb{P}_{nR}$, calculated for experimental parameters typical for Bi-2212 IJJ's. The corresponding quality factors are indicated in the figures. From Fig. 17(a), it is seen that at $T < T^*$, the $\mathbb{P}_{nR} = 1$ in the region where $P_S > 0$; therefore, retrapping is insignificant. However, at $T > T^*$, retrapping becomes significant at small currents. The resulting conditional probability density of measuring the switching current, P_{SR}, Eq. (20), normalized by the total number of switching events, is shown by the solid line in Fig. 17(b). This explains very well both the reduced width and the almost symmetric shape of the measured histogram.

B. Collapse temperature

Figure 19(a) shows the bias dependence of switching ΔU_S and retrapping ΔU_R barriers. As was noted in Ref. 9, there is always a current $I_{R0} < I_e < I_{c0}$ at which $\Delta U_S(I_e) = \Delta U_R(I_e)$, so that switching and retrapping processes become equally probable. However, this will have an influence on the switching current statistics only in the case when the probability density of switching at this current is considerable. For the case $Q_0 = 3$, shown in Fig. 19(a), $I_e / I_{c0} \simeq 0.7$. However, at low T, the major part of switching events will occur at $I_{Smax} \simeq I_{c0} > I_e$. Such a situation is seen in Fig. 17(a) for $T < T^*$: the probability of not being retrapped, $\mathbb{P}_{nR} \simeq 1$, at the most probable switching current I_{Smax} and according to the criterion, Eq. (20), retrapping has no influence on the switching statistics.

Figure 19(b) and 19(c) represent numerical simulations in which we intentionally disregarded T dependencies of $I_{c0} = 20$ μA, Q_0, and E_{J0} for simplicity of analysis. Parameters were chosen similar to that for the S-2DEG-S 2b at $H = 3.66$ μT, see Fig. 9. The two considered cases correspond to the estimated capacitance of junction 2b ($Q_0 = 1.373$) and twice the capacitance ($Q_0 = 1.942$), respectively. From Fig. 19(b), it is seen that the most probable switching current I_{Smax} decreases, while the most probable retrapping current I_{Rmax} increases with T as a result of thermal fluctuations. The widths of both switching ΔI_S and retrapping ΔI_R histograms continuously increase with T for conventional TA, as seen from Fig. 19(c). As expected, switching histograms are unaffected by the small variation of Q_0, so that both I_{Smax} and ΔI_S coincide for the two values of Q_0. On the contrary, retrapping histograms are strongly affected by Q_0: the $I_{Rmax}(T)$ dependence becomes weaker and ΔI_R smaller with increasing Q_0. This is caused by the increase of the retrapping barrier ΔU_R with Q_0 as seen from Fig. 19(a).

Since I_{Smax} decreases while I_{Rmax} increases with T, switching and retrapping histograms inevitably will overlap at a certain temperature T^*. Figures 19(b) and 19(c) clearly demonstrate that the collapse of thermal fluctuations of the measured switching current ΔI occurs at T^* and that the T^* itself strongly depends on Q_0. From the simulations presented in Fig. 19, it is clear that the collapse is not caused by a crossover from underdamped to overdamped state since Q_0 was T independent in this case.

The collapse temperature can be estimated from the following system of equations:

$$\Gamma_{TA}(I_{Smax}) \simeq (dI/dt)/I_{c0}, \qquad (21)$$

$$\Gamma_R(T^*, I_{Smax}) = \Gamma_{TA}(T^*, I_{Smax}). \qquad (22)$$

Equation (21) states that the JJ switches into the R state during the time of the experiment. From Eqs. (2) and (21), it follows that

$$\frac{\Delta U_S(I_{Smax})}{k_B T} \simeq \ln\left[\frac{a_t \omega_p I_{c0}}{2\pi(dI/dt)}\right] \equiv Y. \qquad (23)$$

In the measurements presented here, $Y \simeq 24$, as seen from the inset of Fig. 20. The parameter Y is weakly (logarithmically) dependent on experimental parameters and, therefore, has approximately the same value in different studies of switching statistics of JJ's. From Eqs. (3) and (23), we obtain the value of the most probable switching current I_{Smax} (disregarding retrapping):

$$I_{Smax}/I_{c0} \simeq 1 - [T/T_J]^{2/3}, \qquad (24)$$

where $T_J = (4\sqrt{2}E_{J0})/(3Yk_B)$. This dependence is shown by the dashed line in Fig. 19(b) and agrees with numerical simulations (squares).

Similarly, the most probable retrapping current I_{Rmax} (disregarding switching) is obtained from Eqs. (7), (22), and (23):

$$I_{Rmax} \simeq I_{R0} + I_{c0}\sqrt{\frac{2k_B T(Y+X)}{E_{J0}Q_0^2}}, \qquad (25)$$

where $X = \ln\left[\frac{2\pi(I_{Smax}-I_{R0})}{a_t I_{c0}(1-(I_{Smax}/I_{c0})^2)^{1/4}}\sqrt{\frac{E_{J0}}{2\pi k_B T}}\right]$ is the logarithm of the ratio of prefactors of TA retrapping and switching rates, Eqs. (2) and (7). The factor X is only weakly dependent on experimental parameters and, in the first approximation, can be considered constant (or even neglected). For the case of S-2DEG-S 2b, $X \simeq 3$. Red dashed lines in Fig. 19(b) represent $I_{Rmax}(T)$ calculated from Eq. (25) with $Y = 24$ and $X = 3$, which perfectly reproduce the simulated $I_{Rmax}(T)$ for both Q_0 values.

Knowing $I_{Smax}(T)$ and $I_{Rmax}(T)$, we can easily obtain T^* from the condition [cf. Figs. 19(b) and 19(c)]:

$$I_{Rmax}(T^*) = I_{Smax}(T^*). \qquad (26)$$

A simple analytic estimation of T^* can be obtained by observing that $I_{Smax}(T)$ is almost linear in a wide T range, as seen from Figs. 19(b) and 11. In this case, Eq. (24) can be approximated as

$$I_{Smax}/I_{c0}^* \simeq 1 - \beta T, \qquad (27)$$

where $\beta = 2/(3T_J^{2/3}T_0^{1/3} - T_0)$, $I_{c0}^* = I_{c0}[1 - (T_0/T_J)^{2/3}/3]$, and T_0 is some characteristic temperature $\sim T_J$. Substituting Eq. (27) into Eq. (26), taking a simple approximation for I_{R0}, Eq. (7), and neglecting T dependence of I_{c0}, we obtain a quadratic equation for T^*, which yields

$$T^* \simeq \frac{k_B(Y+X)}{2\beta^2 E_{J0}Q_0^2}\left[\sqrt{1 + \left(\frac{I_{c0}^*}{I_{c0}} - \frac{4}{\pi Q_0}\right)\frac{2Q_0^2 \beta E_{J0}}{k_B(Y+X)}} - 1\right]^2. \qquad (28)$$

From Eq. (28), it follows that $k_B T^*/E_{J0}$ strongly depends on Q_0 but is independent of E_{J0} because T appears in Eqs. (21) and (25) only in combination T/E_{J0} [in the case of Eq. (28) because $\beta \sim 1/E_{J0}$].

The dashed line in the main panel of Fig. 20 represents the numerically simulated T^* normalized by E_{J0} and I_{c0} (left and right axes, respectively) as a function of the quality factor Q_0. It was obtained by numerical solution of Eq. (26), without simplifications used for the derivation of Eq. (28). For overdamped JJ's, $Q_0 < 0.84$, $T^*/I_{c0} \to 0$. The T^*/I_{c0} continuously grows with increasing $Q_0 > 0.84$ and saturates at ~ 2 K/μA for strongly underdamped JJ's, $Q_0 \gg 1$.

The symbols in Fig. 20 represent experimental values of T^*/I_{c0} for the JJ's studied in this work. The experimental data agree well with the proposed theory (dashed line). The simulated values of T^*/I_{c0} are also consistent with experimental data for underdamped SIS-type JJ's Al-AlO$_x$-Al, $T^*/I_{c0} \simeq 1-3.3$ K/μA,[1] and Nb-AlO$_x$-Nb, $T^*/I_{c0} \simeq 1$ K/μA (Ref. 3) [with a reservation that these measurements were done on SQUID's, which may have different activation energies than single JJ's, Eqs. (3) and (8)].

The T^*/I_{c0} dependence, shown by the dashed line in Fig. 20, is almost universal and explains the paradoxical collapse of switching current fluctuations, reported in Refs. 1–3, as well as the data presented here. For example, recovery of conventional TA switching in C-shunted S-2DEG-S junctions, see Fig. 18, is caused by the increase of the Q_0, which, according to Fig. 20, results in larger T^* for the same I_{c0}. Similarly, the decrease of Q_0 due to suppression of I_{c0} causes the collapse of switching histograms as a function of V_g in Fig. 14 and the decrease of T^* with H in Fig. 15.

From Fig. 20, it is seen that in overdamped junctions, $T^* = 0$, implying that retrapping is crucially affecting switching statistics at any T. In this case, $T_{esc}(T)$ and $\Delta I(T)$ decrease at all T. We observed such behavior for S-2DEG-S junctions with small I_{c0} and, consequently, small Q_0. The tendency of decreasing T^* with decreasing I_{c0} is apparent from Fig. 15(a).

Therefore, observation of the collapse, i.e., a maximum of $T_{esc}(T)$ at $T^* > 0$, is the most unambiguous indication of underdamped, $Q_0 > 0.84$, state in the studied JJ's. The estimation of Q_0 from the value of T^* confirms our assessment of junction capacitances, made in Sec. IV.

C. Phase dynamics in the collapsed state

The insight into the phase dynamics at $T > T^*$ can be obtained from the inset of Fig. 20, in which the dependence of $\Delta U_S(I = I_{Smax})$ vs T is shown for the case of Fig. 15(a). The dashed line corresponds to $\Delta U_S(I_{Smax})/k_B T = 24.3 \simeq Y$ obtained from simulations presented in Fig. 19 and demonstrates excellent agreement with the experiment. The large value of $\Delta U_S/k_B T$ implies that the JJ can escape from the S to the R state only a few times during the time of the experiment. Therefore, the collapse is not due to transition into the phase-diffusion state, which may also lead to reduction of ΔI.[14] Indeed, phase diffusion requires repeated escape and retrapping, which is only possible for $\Delta U_S/k_B T \sim 1$.[9,55] Careful measurements of supercurrent branches in the IVC's at $T \gtrsim T^*$ did not reveal any dc voltage down to ~ 10 nV for S-2DEG-S JJ's and ~ 1 μV for IJJ's. Furthermore, the IVC's

remain hysteretic at $T > T^*$, which is incompatible with the phase diffusion within the RCSJ model.[9] As can be seen from Fig. 10, the phase diffusion in IJJ's appears only at $T > 90$ K, meaning that all the collapse shown in Fig. 13(b) at 75 K $< T <$ 85 K occurs *before* entering into the phase-diffusion state.

Therefore, in the collapse state, the junction makes a few very short excursions from the S to the R state during the current sweep, before it eventually switches into the R state. However, the number of excursions and the total excursion time are so small that they do not lead to a measurable dc voltage in the JJ. The occurrence of the corresponding phase dynamic state, prior to the phase diffusion, has been observed by numerical modeling and discussed in Ref. 9.

VII. CONCLUSIONS

We have analyzed the influence of damping on the switching current statistics of moderately damped Josephson junctions, employing a variety of methods for accurate tuning of the damping parameter. A paradoxical collapse of switching current fluctuations with increasing temperature was observed in various types of Josephson junctions,[1–3] including low-T_c SNS, SFS, S-2DEG-S, SIS, and high-T_c intrinsic Josephson junctions. The unusual phenomenon was explained by an interplay of two conflicting consequences of thermal fluctuations, which, on one hand, assist in premature switching to the R state and, on the other hand, help in retrapping back into the S state. In this case, the probability of measuring a switching event becomes a conditional probability of switching and not being retrapped during the time of the experiment. Numerical calculations have shown that this model provides a quantitative explanation of both the value of the collapse temperature T^* and the unusual shape of switching histograms in the collapsed state. Based on the theoretical analysis, we conclude that the collapse represents a very general phenomenon which must occur in any underdamped JJ at sufficiently high T.

The collapse of switching current fluctuations in Josephson junctions represents an exception from the law of increasing of thermal fluctuations with temperature. In the studied case, the "failure" of this general law of nature is caused by the coexistence of two counteracting processes (switching and retrapping). It should be emphasized that fluctuations for each of the two processes alone follow the law and enhance with T in a conventional manner. It is, however, remarkable and unusual that fluctuations may cancel each other out and lead to reduction of thermal fluctuations of a physically measurable quantity.

Finally, we note that the reduced width of switching histograms in the collapsed state of moderately damped JJ's may be advantageous for single-shot readout of superconducting qubits,[56] which requires accurate discrimination of two close current states.

[1] J. M. Kivioja, T. E. Nieminen, J. Claudon, O. Buisson, F. W. J. Hekking, and J. P. Pekola, Phys. Rev. Lett. **94**, 247002 (2005).

[2] V. M. Krasnov, T. Bauch, S. Intiso, E. Hürfeld, T. Akazaki, H. Takayanagi, and P. Delsing, Phys. Rev. Lett. **95**, 157002 (2005).

[3] J. Männik, S. Li, W. Qiu, W. Chen, V. Patel, S. Han, and J. E. Lukens, Phys. Rev. B **71**, 220509(R) (2005).

[4] P. Hänggi, P. Talkner, and M. Borkovec, Rev. Mod. Phys. **62**, 251 (1990).

[5] A. O. Caldeira and A. J. Leggett, Phys. Rev. Lett. **46**, 211 (1981).

[6] E. Ben-Jacob, D. J. Bergman, B. J. Matkowsky, and Z. Schuss, Phys. Rev. A **26**, 2805 (1982).

[7] H. Grabert, P. Olschowski, and U. Weiss, Phys. Rev. B **36**, 1931 (1987).

[8] J. M. Martinis and H. Grabert, Phys. Rev. B **38**, 2371 (1988).

[9] R. L. Kautz and J. M. Martinis, Phys. Rev. B **42**, 9903 (1990).

[10] S. Washburn, R. A. Webb, R. F. Voss, and S. M. Faris, Phys. Rev. Lett. **54**, 2712 (1985).

[11] J. M. Martinis, M. H. Devoret, and J. Clarke, Phys. Rev. B **35**, 4682 (1987).

[12] P. Silvestrini, S. Pagano, R. Cristiano, O. Liengme, and K. E. Gray, Phys. Rev. Lett. **60**, 844 (1988).

[13] E. Turlot, D. Esteve, C. Urbina, J. M. Martinis, M. H. Devoret, S. Linkwitz, and H. Grabert, Phys. Rev. Lett. **62**, 1788 (1989).

[14] D. Vion, M. Gotz, P. Joyez, D. Esteve, and M. H. Devoret, Phys. Rev. Lett. **77**, 3435 (1996).

[15] M. G. Castellano, R. Leoni, G. Torrioli, F. Chiarello, C. Cosmelli, A. Costantini, G. Diambrini-Palazzi, P. Carelli, R. Cristiano, and L. Frunzio, J. Appl. Phys. **80**, 2922 (1996); M. G. Castellano, G. Torrioli, F. Chiarello, C. Cosmelli, and P. Carelli, *ibid.* **86**, 6405 (1999).

[16] M. Schlosshauer, Rev. Mod. Phys. **76**, 1267 (2004).

[17] R. McDermott, R. W. Simmonds, M. Steffen, K. B. Cooper, K. Cicak, K. D. Osborn, S. Oh, D. P. Pappas, and J. M. Martinis, Science **307**, 1299 (2005); A. J. Berkley, H. Xu, R. C. Ramos, M. A. Gubrud, F. W. Strauch, P. R. Johnson, J. R. Anderson, A. J. Dragt, C. J. Lobb, and F. C. Wellstood, *ibid.* **300**, 1548 (2003).

[18] I. Chiorescu, P. Bertet, K. Semba, Y. Nakamura, C. J. P. M. Harmans, and J. E. Mooij, Nature (London) **431**, 159 (2004).

[19] D. Vion, A. Aassime, A. Cottet, P. Joyez, H. Pothier, C. Urbina, D. Esteve, and M. H. Devoret, Science **296**, 886 (2002); Yu. A. Pashkin, T. Yamamoto, O. Astafiev, Y. Nakamura, D. V. Averin, and J. S. Tsai, Nature (London) **421**, 823 (2003).

[20] T. Bauch, T. Lindström, F. Tafuri, G. Rotoli, P. Delsing, T. Claeson, and F. Lombardi, Science **311**, 57 (2006).

[21] The prefactor γ leads to thermal enhancement of the MQT escape rate. The enhancement depends on damping and is insignificant for underdamped JJ's, see, e.g., Fig. 11 of Ref. 7.

[22] K. K. Likharev, *Dynamics of Josephson Junctions and Circuits* (Gordon and Breach, New York, 1991).

[23] The same result could also be derived from the expression $d\mathbb{P}_0/dt = -\Gamma_{01}\mathbb{P}_0$, valid for arbitrary initial $\mathbb{P}_0$ at $t=0$.

[24] A. A. Golubov, M. Yu. Kupriyanov, and E. Ilichev, Rev. Mod. Phys. **76**, 411 (2004); T. Bauch, F. Lombardi, F. Tafuri, A. Barone, G. Rotoli, P. Delsing, and T. Claeson, Phys. Rev. Lett. **94**, 087003 (2005).

[25] NbCuNi bilayers were made by V. A. Oboznov at the Institute of Solid State Physics, Chernogolovka, Russia.

[26] V. M. Krasnov, O. Eriksson, S. Intiso, P. Delsing, V. A. Oboznov, A. S. Prokofiev, and V. V. Ryazanov, Physica C **418**, 16 (2005).

[27] Nb/Pt/Nb trilayers were made by H. Frederiksen at Chalmers University of Technology, Gothenburg, Sweden.

[28] T. Golod, M.S. thesis, Chalmers University of Technology, 2005.

[29] S-2DEG-S junctions were provided by T. Akazaki and H. Takayanagi from the NTT Basic Research Laboratories, Kanagawa, Japan.

[30] H. Takayanagi, T. Akazaki, and J. Nitta, Phys. Rev. Lett. **75**, 3533 (1995); T. Akazaki, H. Nakano, J. Nitta, and H. Takayanagi, Appl. Phys. Lett. **86**, 132505 (2005).

[31] T. Bauch, E. Hürfeld, V. M. Krasnov, P. Delsing, H. Takayanagi, and T. Akazaki, Phys. Rev. B **71**, 174502 (2005).

[32] R. Kleiner and P. Müller, Phys. Rev. B **49**, 1327 (1994).

[33] V. M. Krasnov, A. Yurgens, D. Winkler, P. Delsing, and T. Claeson, Phys. Rev. Lett. **84**, 5860 (2000); V. M. Krasnov, A. E. Kovalev, A. Yurgens, and D. Winkler, *ibid.* **86**, 2657 (2001).

[34] V. M. Krasnov, Phys. Rev. B **65**, 140504(R) (2002).

[35] V. M. Krasnov, N. Mros, A. Yurgens, and D. Winkler, Phys. Rev. B **59**, 8463 (1999).

[36] A. Irie, Y. Hirari, and G. Oya, Appl. Phys. Lett. **72**, 2159 (1998); Yu. I. Latyshev, A. E. Koshelev, V. N. Pavlenko, M. B. Gaifullin, T. Yamashita, and Y. Matsuda, Physica C **367**, 365 (2002); S. M. Kim, H. B. Wang, T. Hatano, S. Urayama, S. Kawakami, M. Nagao, Y. Takano, T. Yamashita, and K. Lee, Phys. Rev. B **72**, 140504(R) (2005).

[37] K. Inomata, S. Sato, K. Nakajima, A. Tanaka, Y. Takano, H. B. Wang, M. Nagao, H. Hatano, and S. Kawabata, Phys. Rev. Lett. **95**, 107005 (2005); X. Y. Jin, J. Lisenfeld, Y. Koval, A. Lukashenko, A. V. Ustinov, and P. Müller, *ibid.* **96**, 177003 (2006).

[38] V. M. Krasnov, T. Bauch, and P. Delsing, Phys. Rev. B **72**, 012512 (2005).

[39] The studied Bi-2212 structure had a triple-mesa configuration, containing two contact mesas on top of a common pedestal. This allowed four-probe measurement of IJJ's in the pedestal mesa, shown in Fig. 10. The switching statistics in Figs. 11, 13, and 17 was obtained from a stable switching of one of the IJJ's from the contact mesa. Since contact mesas had approximately two times smaller area than the pedestal mesa, IJJ's in the contact mesa had approximately two times smaller critical current, as seen from comparison of Figs. 10 and 11. More details about triple mesa structures can be found in V. M. Krasnov, Phys. Rev. Lett. **97**, 257003 (2006).

[40] A. T. Johnson, C. J. Lobb, and M. Tinkham, Phys. Rev. Lett. **65**, 1263 (1990).

[41] T. A. Fulton and L. N. Dunkleberger, J. Appl. Phys. **45**, 2283 (1974); W. J. Skocpol', M. R. Beasley, and M. Tinkham, *ibid.* **45**, 4054 (1974).

[42] Y. Song, J. Appl. Phys. **47**, 2651 (1976).

[43] V. M. Krasnov, M. Sandberg, and I. Zogaj, Phys. Rev. Lett. **94**, 077003 (2005).

[44] V. M. Krasnov, V. A. Oboznov, and V. V. Ryazanov, Physica C **196**, 335 (1992).

[45] V. M. Krasnov, N. F. Pedersen, V. A. Oboznov, and V. V. Ryazanov, Phys. Rev. B **49**, 12969 (1994).

[46] V. M. Krasnov, N. F. Pedersen, and V. A. Oboznov, Phys. Rev. B **50**, 1106 (1994).

[47] I. Zutic, J. Fabian, and S. Das Sarma, Rev. Mod. Phys. **76**, 323 (2004).

[48] A minor decrease of resistance of C-shunted S-2DEG-S JJ's is probably associated with the removal of the Al-gate electrode from the top of the semiconducting heterostructure during the C-shunt fabrication. This removes the Schottky barrier present below the gate electrode in the unshunted JJ.

[49] B. Bayraktaroglu, J. Barrette, L. Kehias, C. I. Huang, R. Fitch, R. Neidhard, and R. Scherer, IEEE Electron Device Lett. **14**, 493 (1993).

[50] V. M. Krasnov, A. Yurgens, D. Winkler, and P. Delsing, J. Appl. Phys. **89**, 5578 (2001); **93**, 1329 (2003).

[51] V. M. Krasnov, V. A. Oboznov, V. V. Ryazanov, N. Mros, A. Yurgens, and D. Winkler, Phys. Rev. B **61**, 766 (2000).

[52] P. A. Warburton, A. R. Kuzhakhmetov, O. S. Chana, G. Burnell, M. G. Blamire, H. Schneidewind, Y. Koval, A. Franz, P. Muller, D. M. C. Hyland, D. Dew-Hughes, H. Wu, and C. R. M. Grovenor, J. Appl. Phys. **95**, 4941 (2004).

[53] N. Mros, V. M. Krasnov, A. Yurgens, D. Winkler, and T. Claeson, Phys. Rev. B **57**, R8135 (1998).

[54] V. M. Krasnov and D. Winkler, Phys. Rev. B **56**, 9106 (1997).

[55] A. Franz, Y. Koval, D. Vasyukov, P. Muller, H. Schneidewind, D. A. Ryndyk, J. Keller, and C. Helm, Phys. Rev. B **69**, 014506 (2004).

[56] C. H. Van der Wal, F. K. Wilhelm, C. J. P. M. Harmans, and J. E. Mooij, Eur. Phys. J. B **31**, 111 (2003).